Realization of negative refractive index with double-layered H-shaped resonator array

Xiang Xiong,[1] Zhao-Wu Wang,[1] Shao-Jie Fu,[1] Mu Wang,[1,a)] Ru-Wen Peng,[1] Xi-Ping Hao,[1] and Cheng Sun[2]
[1]*National Laboratory of Solid State Microstructures and Department of Physics, Nanjing University, Nanjing 210093, China*
[2]*Department of Mechanical Engineering, Northwestern University, Evanston, Illinois 60208-3111, USA*

(Received 14 August 2011; accepted 9 October 2011; published online 3 November 2011)

With an assembly of double-layered H-shaped metallic resonators, we simultaneously realized both magnetic and electric resonances at the same frequency band. Negative refractive index (NRI) is consequently achieved. The frequency band with NRI can be tuned by the structural parameters of the H-shaped resonators. This design demonstrates a unique example to construct metamaterial with NRI feature. © *2011 American Institute of Physics*. [doi:10.1063/1.3656715]

Metamaterial opens a new gateway to achieve some electromagnetic properties that do not exist in nature, including negative refractive index (NRI)[1–4] and invisible cloaking,[5–7] etc. For the negative refractive index, early designing follows the idea to combine a resonant magnetic structure with another metallic structure that provides a "background" of negative permittivity in a broad spectral range.[8–11] In other words, the frequency of magnetic resonance is imbedded in a broader spectral range where electric resonance exists. We once proposed an assembly of double-layered metallic U-shaped resonators (USRs), which possesses pure electric and magnetic responses at different frequencies, leading to both negative permeability and permittivity.[12] With USRs, the magnetic and electric resonances can be interchanged at nearly the same frequency by simply rotating the polarization of incident light for 90°. This means if we keep the polarization of incident light and rotate each neighboring USRs for 90°, negative permeability and negative permittivity can be simultaneously realized at the same frequency. In other words, with proper assembly of the same type of building blocks, it is possible to achieve the negative refractive index. Up to now, a number of structures have been proposed in order to attain negative refractive index, such as fishnets,[4,11] short wire pairs,[13] or split rings,[1,14] to name a few. Here, we demonstrate that with an array of double-layered H-shaped resonators (HSRs), magnetic and electric resonances can be simultaneously activated at the same frequency. Consequently, negative refractive index can be realized.

The building block of our design consists of two types of double-layered H-shaped metallic resonators. As indicated in Fig. 1(a), in the stacked HSRs, the upper structure is orthogonally rotated with respect to that on the lower layer. We denote one configuration as H_1 (Fig. 1(b), left), and its mirror-imaged counterpart as H_2 (Fig. 1(b), right). Thereafter, we combine H_1 and H_2 into a 2×2 basic unit, as shown in Fig. 1(c). It should be pointed out that each HSR is not symmetric in geometry, i.e., the short metallic bar perpendicularly positioned in between two longer parallel bars in the H pattern is not exactly at the middle of the structure. Instead, it has been deviated from the geometrical center for 0.3 μm in our case. The 2×2 basic building units are arranged in a simple square lattice. The coordinate frame is so set that the diagonal directions of HSRs are defined as $\boldsymbol{x}$ and $\boldsymbol{y}$ directions, respectively, as shown in Figs. 1(b) and 1(c). The incident light comes along $+\boldsymbol{z}$ direction and is either $\boldsymbol{x}$-polarized or $\boldsymbol{y}$-polarized. In the simulation, the ambient environment is set as vacuum.

Commercial software (CST) based on the finite difference time domain (FDTD) method has been applied to calculate the transmission/reflection coefficients for both $\boldsymbol{x}$- and $\boldsymbol{y}$-polarized incident light. In the calculation, the permittivity of gold in the infrared regime is based on Drude model, $\varepsilon(\omega) = 1 - \omega_p^2/(\omega^2 + i\omega_\tau\omega)$, where ω_p is the plasma frequency and ω_τ is the damping constant. For gold, these characteristic frequencies are taken as $\omega_p = 1.37 \times 10^4$ THz and $\omega_\tau = 40.84$ THz, respectively.[15] Considering that the electrons may experience additional scattering from metal surfaces, following Ref. 16, we take the damping constant twice higher than that of the bulk material in the simulation. For $\boldsymbol{x}$-polarized incidence, two evident resonances can be identified in the transmission (dark solid line) and the reflection (dark dashed line) at 550 cm^{-1} and 620 cm^{-1}, respectively. For $\boldsymbol{y}$-polarized incidence, only one resonance is detected in the transmission (light solid line) and the reflection (light dashed line) around 590 cm^{-1}. In the simulation, the polarization of light does not change through the whole process, so the retrieval method based on S-parameters[17] can be safely applied. Figures 2(b)–2(d) illustrate the effective permittivity $\varepsilon_{\mathrm{eff}}$, effective permeability μ_{eff}, and the refractive index $\boldsymbol{n}$ of the structure for $\boldsymbol{y}$-polarized incidence, respectively. For $\boldsymbol{y}$-polarized incidence, resonances in effective permittivity and effective permeability lead to the negative refractive index. For $\boldsymbol{x}$-polarized incidence, the situation is nevertheless different. As shown in Figs. 2(b) and 2(c), the resonances of permittivity and permeability occur at 620 cm^{-1} and 550 cm^{-1}, respectively. In this case, negative refraction cannot be realized. To fulfill the negative refractive index, $\varepsilon_r|\mu| + \mu_r|\varepsilon| < 0$ should be satisfied,[18] which originates from the strong absorption associated with the anomalous dispersion around the frequency of resonance. This scenario exactly occurs for $\boldsymbol{y}$-polarized incidence at 590 cm^{-1}.

a)Author to whom correspondence should be addressed. Electronic mail: muwang@nju.edu.cn.

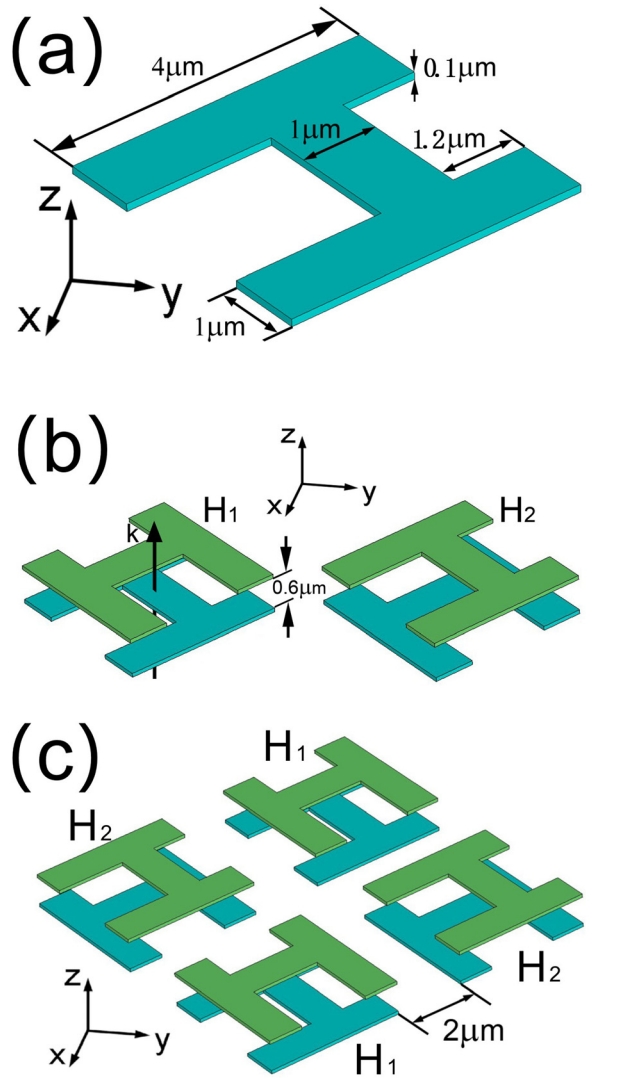

FIG. 1. (Color online) (a) The structure of single layered HSR. (b) The structure of stacked and orthogonally rotated HSR pairs (H_1 and H_2). (c) The 2×2 building unit constructed with H_1 and H_2. The elements in the diagonal directions are identical.

To verify the above numerical calculations, we fabricate HSR array with alignment nesting photolithography. The negative pattern of H-shape array is fabricated on a silicon substrate with photoresist. A 100-nm-thick gold film is then blanket deposited on the patterned substrate, covering the areas with photoresist and the areas where the photoresist has been evacuated (H-shaped pattern). Thereafter, the photoresist is removed with solvent, leaving only gold HSRs on silicon substrate. Then a layer of 600-nm-thick silicon nitride is deposited as a spacer layer. A layer of photoresist is again spin-coated, followed by alignment nesting lithography. The second layer of gold film (100 nm in thickness) is deposited and lift-off procedure is applied to remove the photoresist, leaving only the second layer of gold HSRs. In the fabrication process, each HSR on the upper layer located exactly above the one on the lower layer, yet the orientation of each HSR has being rotated for 90°in a specific way so to form an array of HSRs, as illustrated in Fig. 3(a). The inset of Fig. 3(a) shows the detail morphology of the fabricated structure. For sake of structural symmetry in later optical measurements, a silicon layer (2 μm in thickness) is cap-deposited on sample surface.

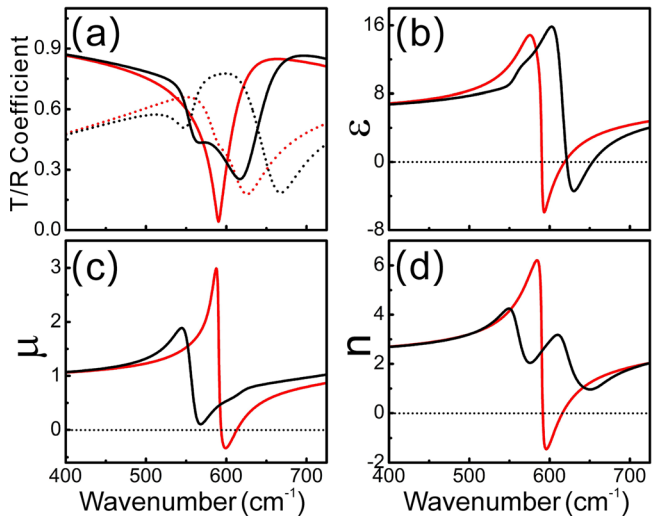

FIG. 2. (Color online) (a) The calculated transmission coefficient (dark solid line) and reflection coefficient (dark dashed line) for ***x***-polarization, and the calculated transmission coefficient (light solid line) and reflection coefficient (light dashed line) for ***y***-polarization. (b) The retrieved effective permittivity and (c) the retrieved permeability for ***x***-polarization (dark solid line) and ***y***-polarization (light solid line). (d) The retrieved refractive index.

The optical property of the fabricated structures is characterized by a vacuum infrared Fourier transform spectrometer (Bruker Vertex 70v), and the setup is schematically shown in Fig. 3(b). In the transmission measurement, the sample is placed between two linear polarizers. Experiments confirm that the polarization of light does not vary in transmission when the incidence is either ***x***- or ***y***-polarized. Figure 3(c) shows the measured transmission spectra for ***x***- and ***y***-polarized incidence. For ***x***-polarized incidence, two resonances are detected at 180 cm^{-1} and 230 cm^{-1}, respectively, in the transmission spectrum (Fig. 3(c), dark line).

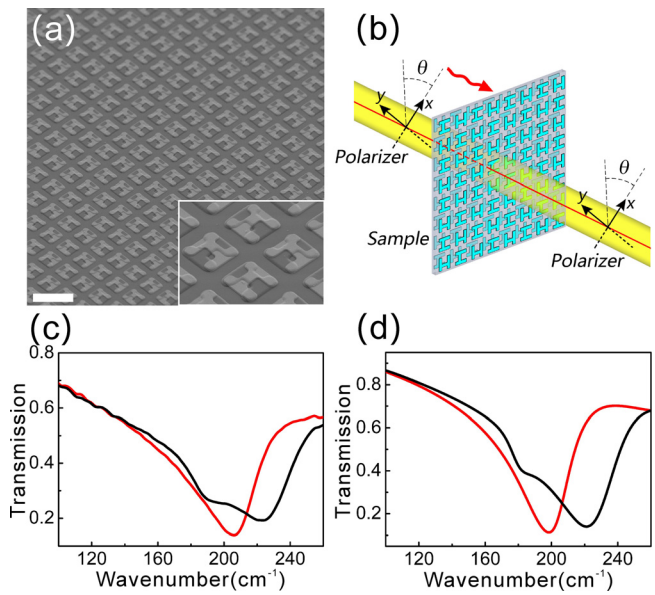

FIG. 3. (Color online) (a) The scanning electron micrograph of the double-layered HSR arrays. The double-layer structure can be easily identified from the inset. The bar stands for 10 μm. (b) The experimental setup of transmission spectra measurement. (c) Experimentally measured transmission and (d) calculated result of the transmission for ***x***-polarized incident light (dark solid line) and ***y***-polarized incident light (light solid line).

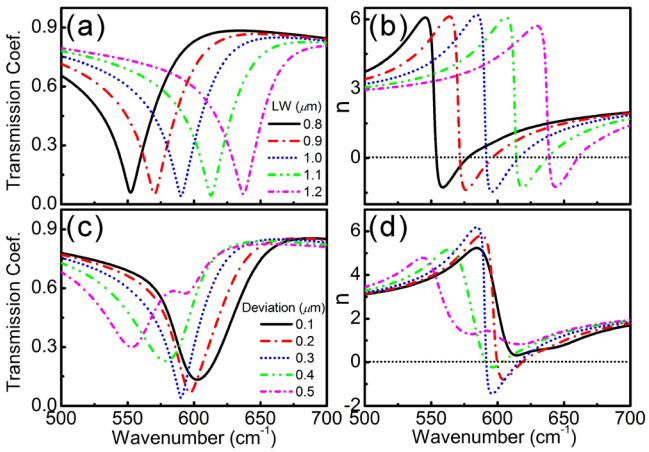

FIG. 4. (Color online) (a) The transmission coefficients and (b) refractive index with *y*-polarization incident for different width of the arms in HSRs. (c) The transmission and (d) refractive index with *y*-polarization incident for different deviation of short metal bar in the H-shape.

For *y*-polarized incidence, only one resonance is observed at $200\,\mathrm{cm}^{-1}$ (Fig. 3(c), light line). In measurement, the phase information cannot be obtained with infrared Fourier transform spectrometer, therefore the refractive index cannot be directly retrieved from the experimental data. However, we can compare the experimentally measured transmission coefficient with the simulated one in Fig. 3(d). It is clear that they are in good agreement. The only difference is that the experimentally observed resonant frequencies for *x*- and *y*-polarized incidence are both lower than that in calculation. This red shift is due to the influence of silicon substrate and silicon nitride spacer in the experimental samples.

To identify the relation of the electric/magnetic resonant frequency and the structural parameters of HSRs, we investigate the change of resonant frequency by fixing the lattice parameters of the array of HSRs, yet changing the width of each arms of HSR. The simulated transmission coefficient and the refractive index are illustrated in Figs. 4(a) and 4(b). By shrinking the width of each arm of HSR, the frequency band corresponding to the negative refractive index shifts to lower frequency. By increasing the width of the arms of HSR, the frequency band with negative refractive index moves to high frequency. This means that one can achieve the negative refractive index at the desired frequency regime by tuning the width of the arms of HSRs.

In our simulation, the short metal bar in H pattern has been deviated from the geometrical center for 0.3 μm. Due to this deviation, the HSR array shows different optical properties for *x*- and *y*-polarization incident. We tune the deviation of the short metal bar in the HSR. Figure 4(c) shows the transmission coefficient of the array of HSRs units with different deviations for *y*-polarized incidence. In Fig. 4(c), one may find that by deviating the short metal bar for 0.1–0.5 μm with respect to the geometrical center, the resonant dip reaches the strongest only when this deviation is 0.3 μm. In Fig. 4(d), the refractive index reaches the most negative value, $n = -1.45$ when the deviation is set as 0.3 μm. When the deviation is 0.2 μm or 0.4 μm, the resonance of transmission becomes weaker and the refractive index becomes less negative. When deviation is 0.1 μm or 0.5 μm, negative refractive index vanishes completely. If the metal bar locates exactly at the middle position (i.e., deviation is zero), the HSR array become optically inactive (polarization-independent). The other extreme scenario is that this short metal bar moves to the end of the perpendicular arms, hence the H-shaped structure turns to the U-shaped structure, which has been studied before.[12] For the U-shaped resonator array, the electric and magnetic resonances occur at different frequencies, and negative refractive index cannot be realized automatically. The deviation of the position of the short metal bar from the end of two parallel bars (U-shape) plays the role to drive the frequencies for electric and magnetic resonances together. This feature is closely related to the material of the substrate. It is noteworthy that we set the deviation of the short metal bar as 0.5 μm in sample fabrication instead of 0.3 μm as that in simulation. This change is for the purpose to overlap the electric and magnetic resonant frequencies, since in real sample fabrication, a silicon substrate and a silicon nitride spacer have to be used. Once the dielectric constant of the substrate becomes lower, the deviation of the short metallic bar will be smaller in order to overlap the two resonant frequencies.

In conclusion, we report here the realization of negative refractive index by tuning the electric and magnetic resonances of the structure to the same frequency. Experimental data are in good agreement with calculations. Although our current structure is designed for infrared frequencies, we anticipate that this principle can be applied to other frequency bands as well. From this point of view, this designing provides a new example to apply split-ring family of metamaterial to realize negative refractive index.

This work was supported by grants from the MOST of China (Grant Nos. 2010CB630705 and 2012CB921502), the NSF of China (Grant Nos. 50972057, 10874068, 11034005, and 61077023), and partly by Jiangsu Province (Grant No. BK2008012).

[1]R. A. Shelby, D. R. Smith, and S. Schultz, Science **292**, 77 (2001).
[2]S. Zhang, W. J. Fan, N. C. Panoiu, K. J. Malloy, R. M. Osgood, and S. R. J. Brueck, Phys. Rev. Lett. **95**, 137404 (2005).
[3]V. M. Shalaev, Nat. Photonics **1**, 41 (2007).
[4]G. Dolling, M. Wegener, C. M. Soukoulis, and S. Linden, Opt. Lett. **32**, 53 (2007).
[5]J. B. Pendry, D. Schurig, and D. R. Smith, Science **312**, 1780 (2006).
[6]D. Schurig, J. J. Mock, B. J. Justice, S. A. Cummer, J. B. Pendry, A. F. Starr, and D. R. Smith, Science **314**, 977 (2006).
[7]R. Liu, C. Ji, J. J. Mock, J. Y. Chin, T. J. Cui, and D. R. Smith, Science **323**, 366 (2009).
[8]G. Dolling, C. Enkrich, M. Wegener, C. M. Soukoulis, and S. Linden, Science **312**, 892 (2006).
[9]K. Lodewijks, N. Verellen, W. Van Roy, V. Moshchalkov, G. Borghs, and P. Van Dorpe, Appl. Phys. Lett. **98**, 091101 (2011).
[10]M. Burresi, D. Diessel, D. van Oosten, S. Linden, M. Wegener, and L. Kuipers, Nano Lett. **10**, 2480 (2010).
[11]J. Valentine, S. Zhang, T. Zentgraf, E. Ulin-Avila, D. A. Genov, G. Bartal, and X. Zhang, Nature **455**, 376 (2008).
[12]X. Xiong, W. H. Sun, Y. J. Bao, R. W. Peng, M. Wang, C. Sun, X. Lu, J. Shao, Z. F. Li, and N. B. Ming, Phys. Rev. B **80**, 201105 (2009).
[13]J. F. Zhou, L. Zhang, G. Tuttle, T. Koschny, and C. M. Soukoulis, Phys. Rev. B **73**, 041101 (2006).
[14]R. Marques, J. Martel, F. Mesa, and F. Medina, Phys. Rev. Lett. **89**, 183901 (2002).
[15]M. A. Ordal, R. J. Bell, R. W. Alexander, L. L. Long, and M. R. Querry, Appl. Opt. **24**, 4493 (1985).
[16]S. Linden, C. Enkrich, M. Wegener, J. F. Zhou, T. Koschny, and C. M. Soukoulis, Science **306**, 1351 (2004).
[17]D. R. Smith, S. Schultz, P. Markos, and C. M. Soukoulis, Phys. Rev. B **65**, 195104 (2002).
[18]R. A. Depine, and A. Lakhtakia, Microw. Opt. Technol. Lett. **41**, 315 (2004).